Make room for iodine: Systematic pore tuning of multivariate metal-organic frameworks for the catalytic oxidation of hydroquinones using hypervalent iodine.

Journal:	*Catalysis Science & Technology*
Manuscript ID	CY-ART-04-2018-000794.R1
Article Type:	Paper
Date Submitted by the Author:	26-Jul-2018
Complete List of Authors:	Tahmouresilerd, Babak; Texas Tech University, Department of Chemistry and Biochemistry Larson, Patrick; Texas Tech University, Department of Chemistry and Biochemistry Unruh, Daniel; Texas Tech University, Chemistry and Biochemistry Cozzolino, Anthony; Texas Tech University, Department of Chemistry and Biochemistry

Catalysis Science & Technology

ARTICLE

Make room for iodine: Systematic pore tuning of multivariate metal-organic frameworks for the catalytic oxidation of hydroquinones using hypervalent iodine.

Received 00th January 20xx,
Accepted 00th January 20xx

DOI: 10.1039/x0xx00000x

www.rsc.org/

Babak Tahmouresilerd, Patrick J. Larson, Daniel K. Unruh and Anthony F. Cozzolino* [a]

Iodine sites have been incorporated in both MIL-53 (Al) and UiO-66 (Zr) MOFs. A multivariate approach was used to increase the accessible area within the pores to allow for the catalytic oxidation of a model substrate, hydroquinone, to the corresponding quinone. In the process, three new phases of MIL-53 were discovered, one of which proved instrumental in allowing catalysis to occur. Both UiO-66 and MIL-53 with 25% incorporated iodine containing linkers allowed for a near-ideal balance between high density of catalytic sites and sufficient space for mass transport to enable catalysis to occur. Good conversions and selectivities were observed in nitromethane, ethyl acetate, acetone and ethanol with UiO-66 which proved to be the more active of the two catalysts. Oxone and 3-chloroperbenzoic acid acted as competent co-oxidants. X-ray photoelectron spectroscopy revealed that the reaction proceeded through an I(III) oxidation state. The MIL-53 framework was readily recycled while the UiO-66 MOF suffered from catalyst deactivation due to particle agglomeration. UiO-66 with 25% iodine containing linker proved to be a competent catalyst for a variety of substituted hydroquinones.

INTRODUCTION

Hypervalent iodine compounds have a variety of applications as stoichiometric or catalytic oxidants in organic synthesis. The development of new hypervalent iodine compounds and the design of enantioselective catalytic systems have been driving forces in the expansion of the field.[1–4] The total synthesis of natural products,[5] oxidative functionalization of unsaturated compounds,[6] oxidative halogenations,[7,8] and oxidation of alcohols[9] are just some of the important applications. Iodine compounds as oxidation catalysts have more recently emerged as an important synthetic tool. In 2005, the oxidative transformations of phenols and α-oxidation of ketones using hypervalent iodine(III) compounds, generated in situ using metachloroperbenzoic acid (mCPBA), were independently reported by Kita[10] and Ochiai.[11] In 2005 and 2006, the catalytic oxidation of primary and secondary alcohols using hypervalent iodine(V) compounds and potassium peroxymonosulfate (Oxone) were independently reported by Vinod[12] and Giannis,[13] respectively. This prompted the exploration of many other catalytic reactions. The advantages of using these hypervalent iodine compounds are their stability toward air and moisture, their commercial availability and the mild reaction conditions.[14,15] They are also considered to be eco-friendly as they circumvent the use of heavy metals.

There are, however, some disadvantages to hypervalent iodine reagents/catalysts. In many cases the hypervalent iodine compound is poorly soluble or completely insoluble in common solvents. The compounds that have been functionalized to improve solubility are not easily recovered and therefore not easily recycled.[16,17,18] Furthermore, in the effort to enhance the functionality of these catalysts to compete with metal-based catalysts, synthetic procedures that involve many steps are often employed.[19,20] Support of hypervalent iodine on polymers has overcome some of these drawbacks by allowing for simple and fast reaction optimization and ready catalyst recovery and reuse.[21–23] The support of hypervalent iodine on polystyrene,[24] silica,[25] macroporous beads,[26] and graphene oxide[27] has also been reported. Indeed, metal nanoparticles were successfully used to make the first hybrid recyclable supports for a hypervalent iodine catalyst.[28] Despite the obvious advantages of these approaches, measuring the molecular weight and appropriate amount of hypervalent iodine compounds can be unclear and the ability to systematically tune these materials can be limited. Furthermore, the geometry around the catalytic site is not clear or static which limits the ability to understand the active site completely. An alternative strategy that seeks to overcome these drawbacks is to support an iodine catalyst in a metal-organic frameworks (MOFs).

Metal-organic frameworks are a class of catalysts that merge the benefits of homogeneous and heterogeneous catalysts.[29] Herein we present a straightforward strategy to incorporate an organic iodine site in a metal-organic framework for catalytic

[a] Department of Chemistry and Biochemistry, Texas Tech University, Box 1061, Lubbock, Texas 79409-1061, United States. Corresponding Author
E-mail: anthony.f.cozzolino@ttu.edu; Fax: +1 806 742 1289; Tel: +1 806 834 1832
Electronic Supplementary Information (ESI) available: Synthesis of MOFs, catalysis conditions, NMR spectra, FTIR spectra, SEM images, single crystal data, powder diffraction data, summary of all reactions, XPS data, DFT Cartesian co-ordinates, DFT vibrational modes and DFT core energies. CCDC: 1578569, 1578119, 1578120. See DOI: 10.1039/x0xx00000x

oxidation. Although inherently insoluble, MOFs have enormous internal surface areas that can facilitate access to a catalytic site. Because of the site-isolation of the iodine, it is not prone to aggregation in a similar manner to molecular hypervalent iodine species such as iodosylbenzene. A variety of factors must be considered in the design including pore shape, pore size, density of catalytic sites, stability of framework, nature of oxidant and shape of the reagent. Our initial targets include the very stable (chemical, thermal and mechanical) MOFs MIL-53 (Al) and UiO-66 (Zr). Importantly, these frameworks do not contain redox active metals that can interfere with the I-mediated catalysis. As shown in Fig. 1, MIL-53 has columnar pores that can change volume due to the breathing nature of this MOF while UiO-66 has rigid tetrahedral and octahedral pores. Using a model reaction, we show that MOF-supported iodine sites are catalytically active and can be easily recovered and reused in certain instances. Here, the approach of making multivariate MOFs (MTV-MOFs) has proved essential to unlocking the reactivity of these systems.

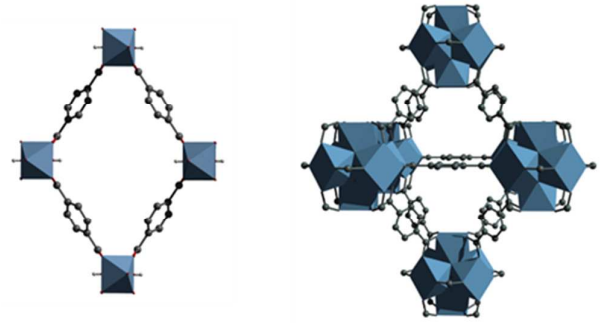

Fig. 1. Depiction of the MIL-53(108.9°) (Al) viewed along (0,1,0) (left), and the octahedral pore in UiO-66 (Zr)[30] (right). Metal coordination spheres are represented with polyhedra. Hydrogen/halogen atoms have been removed for clarity.

RESULTS AND DISCUSSION

Preparation of MOF catalysts

Ultra-stable MOFs UiO-66 and MIL-53 were prepared through modified literature procedures by treating the appropriate metal salt with 1,4-benzenedicarboxylic acid (H_2BDC) derivatives under solvothermal and/or hydrothermal conditions.[31,32] Iodine can be introduced directly into the MOF by substituting 1,4-benzenedicarboxylic acid with 2-iodo-1,4-benzenedicarboxylic acid (H_2IBDC) in the MOF synthesis to give MIL-53 XX%-I or UiO-66 XX%-I, where XX designates the percentage of linker that is $IBDC^{2-}$ and not BDC^{2-}. One critical adaptation was to avoid the use of oxidizing anions, such as nitrates, in the preparation of the MIL-53 MOFs as NMR digestions revealed that the linker no longer matched H_2IBDC which was confirmed by spiking with an authentic H_2IBDC sample. Aluminum chloride hexahydrate or zirconium(IV) chloride served as appropriate metal sources.

Preliminary catalyst evaluation

The oxidation reaction of hydroquinone to benzoquinone (Scheme 1) was chosen as model reaction to evaluate the catalytic behavior of the MOFs prepared with H_2IBDC. Under a typical set of conditions (see Scheme 1), the esterified linker was able to catalyze the oxidation of hydroquinone to benzoquinone with 93% (above the level of the control reaction) conversion and yield. An equivalent experiment with either UiO-66 or MIL-53 100%-I resulted in negligible conversions beyond the level of the control reaction performed in the absence of MOF or with the MOF containing 0%-I (Table 1). Given the good performance of the esterified linker, a likely reason was the inability of the reagents to flow into or out of the framework as a result of the large size of I. The typical approach when such a problem is encountered is to make a longer linker to increase the pore size.[33] An alternative approach is to reduce the density of iodine sites by preparing multivariate MOFs (MTV-MOFs) where some of the $IBDC^{2-}$ linkers are replaced with the smaller BDC^{2-} linkers.

Scheme 1. The oxidation of hydroquinone to benzoquinone shown with typical catalytic conditions.

Table 1. Initial catalytic screening for the oxidation of hydroquinone to benzoquinone by MOF-supported I.[a]

MOF	Conversion (%)b
MIL-53 100%-I	1
UiO-66 100%-I	0
MIL-53 0%-I	-2
UiO-66 0%-I	2
Me_2IBDC	93

a) Reaction conditions: 20 mol% cat., ~2.9 eq. mCPBA, acetonitrile (ACN), 60 min, 50 °C. Values were determined by ^{1}H NMR in the presence of methylsulfonylmethane (MSM) as an internal standard.

b) Reported in excess of the control reaction with no catalyst.

Preparation and characterization of MTV-MOF catalysts

An illustration of the MTV-MOFs with a combination of linkers BDC^{2-} and $IBDC^{2-}$ is shown in Fig. 2. Although the distribution of linkers is random, appropriate ratios of linkers can be selected to maximize the average open space in the pore to facilitate mass transport, while maximizing the density of catalytic sites. Multivariate MIL-53 and UiO-66 (MTV-MIL-53 and MTV-UiO-66) were successfully prepared by adapting literature procedures for the pure linker MOFs.[31,32] Linker ratios of 0, 25, 50, 75 and 100% H_2IBDC:H_2BDC were used.[34] It has been reported that MTV-MOFs do not necessarily incorporate the different linkers in the same ratio that they are added to the reaction mixture.[35] To confirm the ratio of linkers in the MTV-MOFs that were prepared, NMR digestions were performed on all samples. For all MTV-MOFs, the anticipated ratio of linkers, based on reaction stoichiometry, was approximately observed as summarized in Table 2.

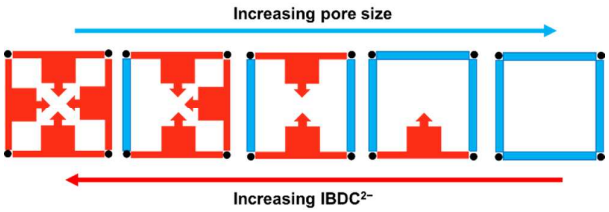

Fig. 2. Illustration of the MTV-MOFs consisting of metal ions or clusters (black circle) coordinated to organic linkers (red arrows for $IBDC^{2-}$ and blue lines for BDC^{2-}).

Table 2. Incorporation of 2-iodoterephthalic acid in MTV-MOFs from ^{1}H NMR digestions.

MTV-MOF	0%-I	25%-I	50%-I	75%-I	100%-I
UiO-66[a]	0	24%	49%	66%	100%
MIL-53[b]	0	19%	45%	73%	100%

a) Digested in 5:1 $(CD_3)_2SO:D_2SO_4$,

b) Digested in 3:1 D_2O:40% NaOD in D_2O.

Thermogravimetric analysis (TGA) was used to establish the thermal stability and the temperature limits for activation and reactions. All frameworks were shown to be stable up to 400 °C (Table S10 and S11). Apart from MTV-MIL-53 (50%-I), a trend of decreasing stability with increasing iodine was observed. The MTV-MIL-53 samples were treated with hot methanol for 16 hours followed by heating at 320 °C for 3 days in order to remove residual materials from the pores. The MTV-UiO-66 samples were activated by washing with hot DMF (x3) and soaking overnight once with hot methanol before filtering and heating at 150 °C for 16 hours under vacuum.

IR spectroscopy was used to probe for the presence of H_2BDC, H_2IBDC or other impurities in the MOF cavities following activation. MIL-53 has been reported to crystallize with free H_2BDC in the pore,[36] and in the case where the free linker is H_2IBDC, this could lead to ready homogeneous catalysis if the linker is not removed prior to catalysis. The FTIR data are in good agreement with reported literature for both MOFs.[31,37] In the case of as-synthesized MTV-MIL-53 MOFs, the peak at 1690 cm^{-1} indicates the presence of free linker within the pores of the framework (Fig. 3). Following activation, this signal was not observed for any multivariate MOFs (Fig. 3). For UiO-66, the peak at 1667 cm^{-1} indicates the presence of residual DMF molecules. These are strongly adsorbed in the framework and are only partially removed upon activation (Fig. 3). No signal could be conclusively identified for the C–I stretching mode, but this vibration is reported to be between 200 and 600 cm^{-1} and DFT calculations predict lower than 300 cm^{-1}, which is outside the mid-IR range (Table S23).

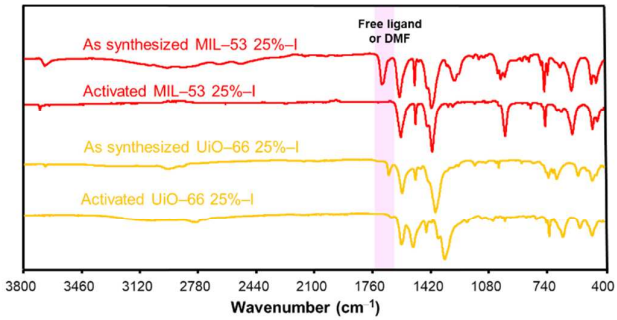

Fig. 3. Di-ATR FTIR of as synthesized and activated MTV-MIL-53 25%-I and MTV-UiO-66 25%-I plotted as attenuation.

Powder x-ray diffraction patterns were obtained for the MTV-MOFs and were compared with the predicted powder patterns of known MOF structures to verify that the anticipated framework was formed. All of the powder x-ray diffraction (PXRD) patterns for the MTV-UiO-66 MOFs are in the good agreement with the simulated pattern of UiO-66.[30] The PXRD patterns of the activated framework revealed that the crystallinity was retained in all cases. For MIL-53, a breathable MOF, the Al–Al–Al angle (see Fig. 4) is used to describe the structures and is denoted as MIL-53(angle). The patterns of the as-synthesized MOFs with 0 and 25% $IBDC^{2-}$ could be matched to the known phase MIL-53(109.8°).[36] After activation, only the MIL-53 0%-I had a powder pattern that corresponded to a narrow pore phase, MIL-53(136.4°).[38] Samples with 25% or more $IBDC^{2-}$ had patterns that were unique from any structure in the Cambridge Structural Database. To ensure that the desired MOF had been prepared, single crystals of MIL-53 100%-I were obtained, and the structure was evaluated. Due to the high level of disorder, the iodine occupancies are less than expected in the single crystal structures, but NMR digestion data of single crystals and bulk powder revealed that only H_2IBCD is present in MIL-53 100%-I (Figure S21). The powder pattern predicted from this phase was found to be in good agreement with the experimental patterns for the as-synthesized MIL-53 with 50-100% I. Two unique phases were found for the activated material; a narrow pore and a large pore phase, MIL-53(124.9°) and MIL-53(108.9°), respectively.

Table 3. MTV-MIL-53 inter-planar angles (assigned from matched PXRD) for the as-synthesized (AS) and activated (AA) form of each phase as a measure of openness of the pores. The radius (r) of cylinder that can fit in the pore is provided in Å in parentheses.[a]

% $IBDC^{2-}$	AS θ (°)	AA θ (°)
0	109.8 (3.2)	136.4 (1.9)
25	109.8 (3.2)	108.9 (3.3)
50	101.3 (3.5)	108.9[b] (3.3)
75	101.3 (3.5)	124.9[b] (2.6)
100	101.3 (3.5)	124.9[b] (2.6)

a) Van der Waals radius of carbon has been subtracted, value assumes benzene rings are tangential to pore.

b) Angle in predominant phase.

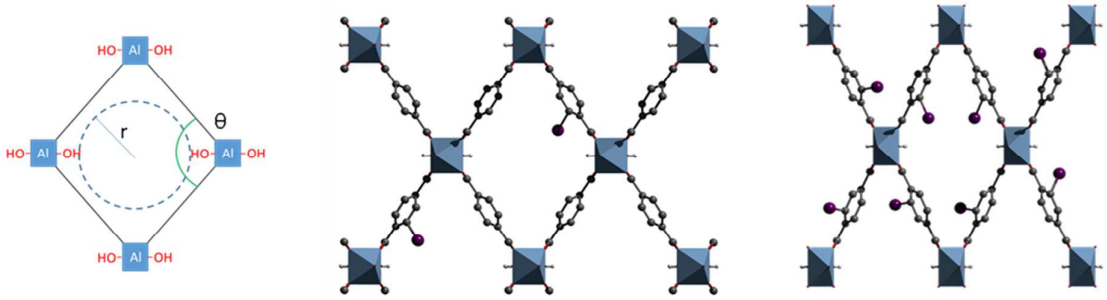

Fig. 4. MTV-MIL-53 pore with interplanar angle and sphere of radius r depicted (left), activated MIL-53 25%-I with Al–Al–Al angle of 108.9° (middle) and activated MIL-53 100%-I with Al–Al–Al angle of 124.9° (right). I atoms are disordered over all sites. A random distribution of I atoms are depicted to match experimental ratio of BDC^{2-}:$IBDC^{2-}$. All structures depicted along (0,1,0). Metal coordination spheres are represented with polyhedra. Hydrogen atoms have been removed for clarity.

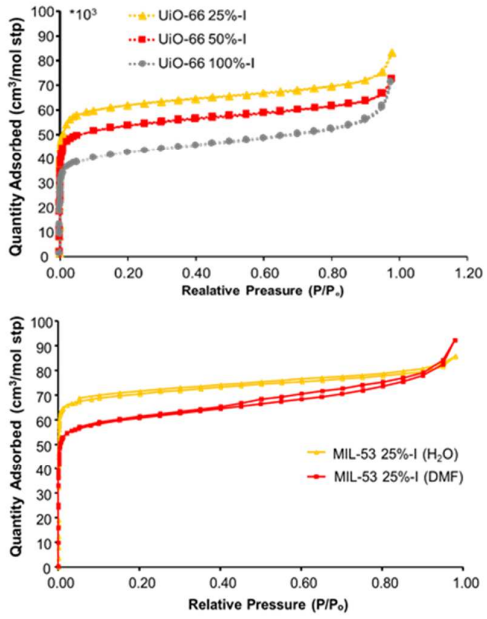

Fig. 5. Nitrogen adsorption isotherms for the MTV-UiO-66 25 (–▲–), 50 (–□–), and 100%-I (–●–) (top) and the MTV-MIL-53 25%-I synthesized with H_2O (–▲–), DMF (–□–) (bottom).

Simulation of the powder patterns reveals that the MIL-53 75%- and 100%-I bulk samples consist primarily of the MIL-53(124.9°) phase. The MIL-53 50%-I bulk powder is also a mix of the two phases, but primarily consists of the larger pore phase MIL-53(108.9°) (Figure S6). The PXRD patterns of the activated MIL-53 25%-I reveal that it only consists of MIL-53(108.9°). MIL-53 can also be prepared solvothermally in N,N-dimethylformamide (DMF) instead of deionized water. A sample of MIL-53 25%-I obtained in this way has the same large pore framework (MIL-53(108.9°), Figure S6). Table 3 describes the Al–Al–Al angles and pore diameters in each of the MIL-53 phases and clearly shows that the MIL-53 25- and 50%-I samples maintain relatively large pores before and after activation, suggesting that the pore will remain open at all points during a reaction.

The effect of iodine on pore size and accessibility can be readily seen from the change in the structure of the MTV-MIL-53 MOFs. With the MTV-UiO-66 frameworks, the effect of the amount of iodine on the internal surface area and pore size can be determined by nitrogen adsorption measurements. MTV-UiO-66 (25, 50, and 100%-I) and MTV-MIL-53 25%-I MOFs show type-I adsorption isotherms (Fig. 5 and Table 4). As the ratio of $IBDC^{2-}$ increases in the frameworks, the molar surface area decreases from the reported value for UiO-66 0%-I (~313000 m^2/mol) as depicted in Fig 5.[32] More important to this study, the pore volume decreases linearly with the increased loading of I to the point where the pores may become inaccessible for substrates/oxidants. The pore volume distributions for UiO-66 25, 50 and 100%-I showed two major pores in the frameworks with pore widths of 6 and 10 Å. As the ratio of the linkers containing I increase in the frameworks, the differential pore volume decreases (Figure S23). In case of multivariate MIL-53 the pore volume distribution revealed that MIL-53 25%-I prepared in DMF has a uniform pore with a width of 6 Å and a higher differential pore volume in the framework when compared to MIL-53 25%-I synthesized hydrothermally.

Table 4. Brunauer-Emmett-Teller (BET) surface areas and pore volumes for the activated UiO-66 25, 50, and 100%-I and MIL-53 25%-I synthesized with water and DMF obtained from nitrogen adsorption isotherms at 77 K.

MOF	BET surface area ($\times 10^3$ $m^2 \cdot mol^{-1}$)[a]	Pore volume (mL/mol)[a]
UiO-66 0%-I[39]	313	120
UiO-66 25%-I	250	117
UiO-66 50%-I	213	103
UiO-66 100%-I	165	93
MIL-53 25%-I (H_2O)	457	173
MIL-53 25%-I (DMF)	447	178

[a] Based on idealized formula and normalized to Zr for UiO-66 and Al for MIL-53.

Catalytic performance of MTV-MOF catalysts in the oxidation of hydroquinone

Catalytic reactions involving these multivariate MOFs revealed that the conversion was strongly dependent on the percentage of $IBDC^{2-}$ in the framework. The oxidation reaction of hydroquinone to benzoquinone under a typical set of conditions (Scheme 1), demonstrated clear catalysis (Table 5). For both MOFs, the yields appear to be inversely proportional

to the amount of incorporated I down to 25% (the lowest % tested, Tables S6 and S7). This was consistent with the increase in internal surface area and pore volume (Fig. 5) for UiO-66. It is also possible that clogging of pore openings by the large I atom plays a role here, particularly for the 50% I (as compared with 25% I) where the surface areas and pore volumes are close. Assuming that the catalysis is occurring in the larger octahedral pore, 25% $IBDC^{2-}$ amounts to 1.5 I sites per pore and represents a near-ideal balance between a high density of catalytic sites and sufficient space for mass transport to efficiently occur. With MIL-53 25%-I the higher yield is attributed to an increase in internal surface area that results from a balance between lower I loading and a more open structure in the breathable MOF. Analysis of the PXRD patterns of the activated and as-synthesized MOFs reveals that MIL-53 25%-I remains in an open and accessible form (angles closest to 90°) under different conditions (Table 3) and therefore has sufficient internal space to facilitate mass transport. Under identical catalytic conditions, no improvement in conversion was observed for MIL-53 25%-I prepared in DMF as opposed to water, but the yield of the desired product increased from 8 to 12%, above the control reaction, suggesting that the MIL-53 25%-I prepared in DMF is more selective. The sizes of the crystalline domains were estimated from the line broadening at the FWHM of the PXRD peaks. Values of 70 nm and 14 nm were obtained for MIL-53 25%-I prepared in water and DMF, respectively. The lack of apparent effect of crystallite size on conversion suggests that the conversion is independent of the particle surface area and that the reaction is occurring inside the pores of the framework rather than on the surface. This is consistent with the differences in reactivity going from 25%-I to 100%-I. The multivariate UiO-66 25%-I and MIL-53 25%-I prepared in DMF were selected for further investigation.

Table 5. Oxidation of hydroquinone to probe the effect of linker ratio in MTV-MOFs.[a]

$IBDC^{2-}$ (%)	Avg. Conversion (%)[b]	
	MIL-53	UiO-66
0%	-2±2	2±1
25%	11±1 (12±3[c])	44±1
50%	4±2	9±2
75%	1±1	11±3
100%	1±1	0±0

a) Reaction conditions: 20 mol% cat., ~2.9 eq. mCPBA, acetonitrile, 60 min and 50 °C. Values were determined by 1H NMR in the presence of MSM as an internal standard.

b) Conversions reported in excess of the control reaction (5%).

c) MIL-53 25%-I prepared in DMF.

To ensure that the catalysis was occurring heterogeneously and not through the leaching of the linker molecule, a split test was performed with both catalysts (Figure S29). Upon removal of the catalysts by a hot filtration no more conversion was observed. This was in contrast to continuing conversion in the samples that remained in the presence of the catalysts. This confirms that the MOF is supporting the catalyst and that the conversion that occurs in excess of the background reaction is occurring heterogeneously.

Iodine is known to function as an oxidant in both the +3 and +5 oxidation states. In order to identify the maximum oxidation state obtained by iodine during catalysis, x-ray photoelectron spectroscopy (XPS) analysis was performed on MIL-53 50%-I and UiO-66 25%-I before and after oxidation with mCPBA. Fig. 6 shows the high resolution I $3d_{5/2}$ XPS signals. The spectra confirm the presence of iodine in two distinct oxidation states (I(I) at 618.5 eV and I(III) at 620.9 eV, Fig. 6). DFT calculations of I(I) and I(III) species revealed a change in chemical shift of ~2 eV between I(I) and I(III), consistent with experiment. I(V) has been reported to have a much higher chemical shift (623.8 eV) then those observed here (Table S24).[40] For MIL-53 50%-I, chemical shifts of 618.5 eV and 620.8 eV were observed both before and after oxidation. An increase in relative intensity was observed for the higher energy shift after oxidation. This suggests that the synthesis or aerobic activation leads to an oxidation of the iodine prior to catalysis. UiO-66 25%-I shows very little oxidized iodine prior to the reaction, but significant amounts following the reaction. These results are consistent with I(III) being the highest attained oxidation state in both materials and with the I(III) acting as the oxidant for the hydroquinones.

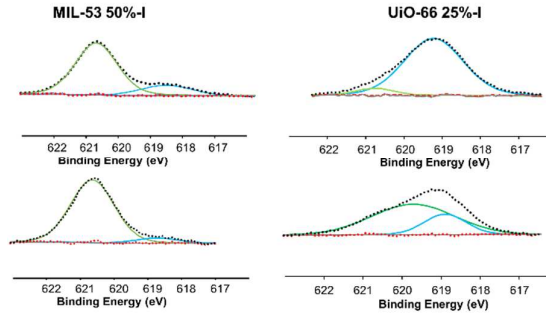

Fig. 6. XPS spectra of I $3d_{5/2}$ region for MTV-MIL-53 50%-I and UiO-66 25%-I before (top) and after (bottom) the oxidation by mCPBA in acetonitrile at 50°C for 5h. Spectra are fitted with two components revealing the presence of two distinct oxidation states.

The choice of solvent can have a significant influence on the reaction. Different solvents were screened under the aforementioned conditions (Fig. 7). The reaction was catalyzed in the presence of acetonitrile, nitromethane, ethyl acetate, acetone, ethanol and methanol; superior conversions to acetonitrile and high selectivities were observed in all solvents for UiO-66 25%-I. In methanol, the catalyst could not be readily evaluated after 60 min due to the high conversion associated with the control reaction. For MIL-53 25%-I, superior conversions were only observed with nitromethane. Lower selectivities were observed with MIL-53 25%-I as compared to UiO-66 25%-I, as other oxidation byproducts (2,5-dihydroxy-1,4-benzoquinone and maleic acid) [41] were observed by ^{1}H NMR.

Reduction of the reaction time to 2 minutes revealed high conversions in nitromethane, ethanol and methanol (Fig. 7) for UiO-66 25%-I. This demonstrates that the MTV-MOFs act as

efficient catalysts, even in methanol. Reduction of the equivalents of co-oxidant in nitromethane revealed no significant change for UiO-66 25%-I but a proportional loss in activity with MIL-53 25%-I (Table S15). Conversely, an increase in equivalents of oxidant used did not increase the conversion in either case, but did increase the conversion in the control reaction.

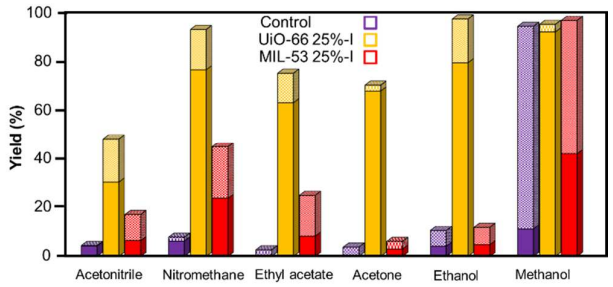

Fig. 7. Catalytic oxidation of hydroquinone to benzoquinone as a function of solvent after 2 minutes (solid color) and 1h (solid + hashed color) with 20 mol% catalyst and 2.9 eq. mCPBA. Values were determined by ^{1}H NMR in the presence of MSM as an internal standard.

Catalytic performance MTV-MOF catalysts in the oxidation of other hydroquinones

The effect of the size and the electronic structure of the substrates was evaluated following the conditions listed in Table 6. The effect of substrate size was evaluated using reactions of hydroquinone and 2,5-di-tert-butylhydroquinone to the corresponding ketones. Due to the lower oxidation potential of these systems,[42] the reactions had to be performed at lower temperatures in order to differentiate the effects of catalysis from the background reaction. In the case of UiO-66 25%-I, a yield of 32% and 54% for hydroquinone and 2,5-di-tert-butylhydroquinone, respectively, were obtained (Entry 2 and 15) which is consistent with 2,5-di-tert-butylhydroquinone being easier to reduce.[39] This contrasts with MIL-53 25%-I which has more restricted pores and has a lower conversion for the larger, easier to oxidize substrate. UiO-66 100%-I gives no conversion beyond the control reaction with both substrates which is consistent with the catalysis occurring within the pores of the MOF, rather than on the external surface (Entry 3, 17). The electronic properties of the substrates in the catalytic reaction were studied by adding the Me and ^{t}Bu as electron donating and Br and Cl as electron withdrawing groups to the substrate with a comparison to the hydroquinone at 24 and 50 ^{o}C, respectively. The catalytic oxidation of substrates containing electron donating groups at 24 ^{o}C showed a better yield of reaction for UiO-66 25%-I when compared to hydroquinone (Entries 9, 12 and 15), consistent with the oxidation potentials.[42] Catalytic oxidations of substrates containing electron withdrawing group at 50 ^{o}C showed a drastic drop from 85% for hydroquinone (Entry 6) to 40% and 67% for 2-chlorohydroquinone and 2,5-dibromohydroquinone, respectively in the presence of UiO-66 25%-I (Entry 19, 22), again consistent with the oxidation potential of these species.[39] Regardless of the oxidation potential of the substrate, the yields were lower with MIL-53 25%-I as compared to hydroquinone, which suggests that size is the predominant determinant with MIL-53 25%-I.

Table 6. Oxidation of hydroquinone derivatives with iodine-functionalized MTV-MOFs.

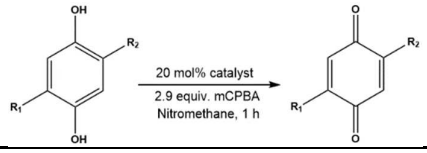

Entry	Substrate		MTV-MOF	Temp. (°C)	Yield (%)[a,b]
	R_1	R_2			
1	H	H	No catalyst	24	3
2			UiO-66 25%-I		35 (32)
3			UiO-66 100%-I		5 (2)
4			MIL-53 25%-I		13 (10)
5	H	H	No catalyst	50	8
6			UiO-66 25%-I		93 (85)
7			MIL-53 25%-I		45 (37)
8	H	Me	No catalyst	24	29
9			UiO-66 25%-I		57 (28)
10			MIL-53 25%-I		36 (7)
11	H	^{t}Bu	No catalyst	24	31
12			UiO-66 25%-I		62 (31)
13			MIL-53 25%-I		34 (3)
14	^{t}Bu	^{t}Bu	No catalyst	24	41
15			UiO-66 25%-I		95 (54)
16			MIL-53 25%-I		43 (2)
17			UiO-66 100%-I		42 (1)
18	H	Cl	No catalyst	50	24
19			UiO-66 25%-I		64 (40)
20			MIL-53 25%-I		44 (20)
21	Br	Br	No catalyst	50	5
22			UiO-66 25%-I		72 (67)
23			MIL-53 25%-I		15 (10)

a) Values were determined by ^{1}H NMR using MSM as an internal standard.

b) The yield of reaction beyond the background reaction is provided in parentheses.

Effect of solvent, co-oxidant and recycling on catalytic oxidation of hydroquinone

The ability to recycle the catalyst was probed using hydroquinone (Fig. 8). In the case of UiO-66 25%-I, the catalytic conversion dropped from 94% to 47% after the first run and finally levelled off at ~30% for the 3rd and 4th cycle, approximately double the control reaction. (Fig. 8, top). These results contrast with the more sluggish MIL-53 25%-I. In nitromethane the conversion and yield held nearly constant over 4 recycles (Fig. 8, bottom). While the small losses in conversion with MIL-53 25%-I could be rationalized as catalyst attrition from manipulations between recycles, the abrupt loss in activity of the UiO-66 catalyst was unexpected and encouraged further study.

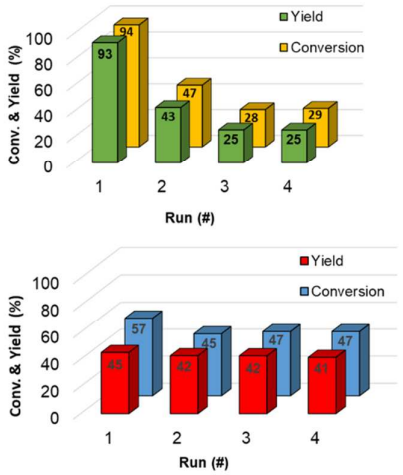

Fig. 8. Recyclability of catalytic conversion after 1 h for hydroquinone to benzoquinone in the presence of MTV-UiO-66 25%-I (top), and MTV-MIL-53 25%-I (bottom). 20 mol% of catalyst, 2.9 eq. mCPBA, nitromethane, 50 °C. Values were determined by ^{1}H NMR in the presence of MSM as an internal standard.

The PXRD patterns for the catalysts after the first and fourth runs were obtained. Fig. 9 and Fig. 10 show that both frameworks retain their crystallinity. Two possible explanations for the loss in reactivity arise: 1) access to either the pores or active sites is being prevented by the accumulation of large organic groups bound to the hypervalent iodine species, or 2) a macroscopic effect such as particle aggregation is occurring and slowing reactivity. Scanning electron microscope (SEM) images of the catalysts before and after the reaction (both were sonicated prior to deposition) revealed that the UiO-66 25%-I particles were aggregating during the reaction (Fig. 11). In contrast, a sample of MIL-53 25%-I treated the same way showed no aggregation. The aggregation of MOF particles has been previously observed and was found to be a function of pH in that case.[43] Here, the acidic oxidant could be having a similar effect. If aggregation is hypothesized to occur by the formation of new metal-linker bonds between particles, one way to prevent this would be to cap the surface metals and replace the surface linkers. To achieve this, UiO-66 25%-I was treated with benzoic acid for 48 h in DMF. The surface-modified MOF was washed, dried and activated to make sure that there is no free ligand or solvent in the pores of the framework. PXRD pattern showed that treated MOF remained crystalline (Figure S30) and digestion analysis confirmed the persistence of 25% 2-iodoterephthalate, and presence of benzoate in the framework (Figure S31). The surface-modified UiO-66 25%-I, however, showed a loss in catalytic activity and selectivity. It is feasible that attempts to surface modify the catalyst may also result in aggregation.

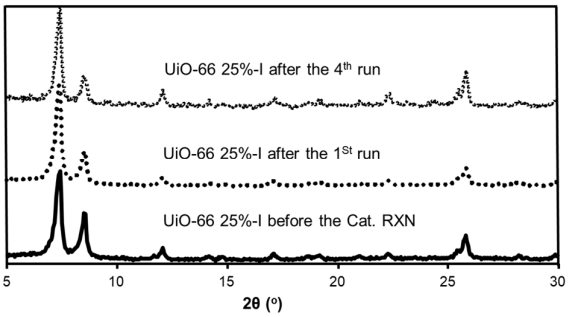

Fig. 9. PXRD patterns of MTV-UiO-66 25%-I before the catalytic reaction, after the first run, and the fourth run

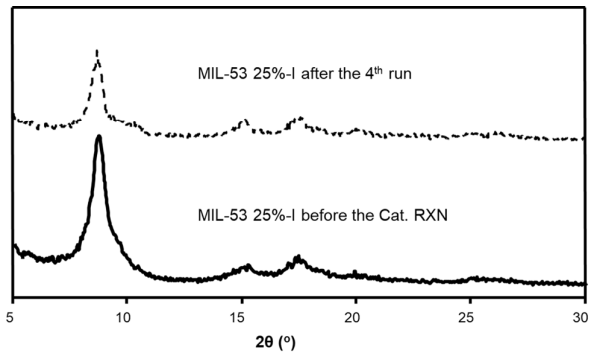

Fig. 10. PXRD patterns of MTV-MIL-53 25%-I before the catalytic reaction and after four cycles.

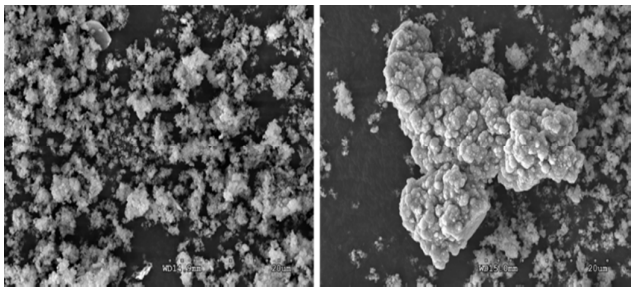

Fig. 11. Scanning electron micrographs of MTV-UiO-66 25%-I before (left) and after (right) the catalytic reactions

While mCPBA is a typical oxidant used with I for catalytic oxidations, a variety of other co-oxidants have been used in the literature.[1] The performance of the catalysts with mCPBA, Oxone, hydrogen peroxide, *tert*-butyl hydroperoxide, and the urea/hydrogen peroxide complex (Hyperol) were tested in a 3:1 nitromethane:water mixture (Tables S16 and S17). With UiO-66 25%-I, good conversions with high selectivities were observed with mCPBA (76% conv. and 75% yield) and Oxone (80% conv. and 78% yield) over 60 min at 50 ℃. With MIL-53 25%-I good conversions with modest selectivities were observed with mCPBA (49% conv. and 37% yield) and Oxone (86% conv. and 70% yield).

Table 7. Catalyst mol% variation for catalytic oxidation of hydroquinone (HQ) to benzoquinone (BQ)

Entry	Catalyst Loading (mol %)	MTV-MOF	Yield (%)
1	20	UiO-66 25%-I	78
2	10		77
3	5		51
4	1		31
5	20	MIL-53 25%-I	70
6	10		45
7	5		34
8	1		23
9	-	No Catalyst	0

Reaction conditions: ~4 eq. oxone, nitromethane/water (3:1 v:v), 60 min and 50 °C. Values were determined by ^{1}H NMR in the presence of MSM as an internal standard.

With Oxone, the catalyst loading with UiO-66 25%-I could be reduced to 10% with no change in the outcome of the reaction over the course of 60 minutes. Further reduction in catalyst loading to 5 and 1% reduced the yields/conversions to 51/67% and 31/49%, respectively. With MIL-53 25%-I the yield/conversions decreased linearly with the catalyst loading (Table 7).

Comparison with related systems

Table 8 compares the oxidation of hydroquinone with a variety of aryl or alkyl hypervalent iodine reagents or catalysts. Iodosyl benzene has the lowest conversion at the highest temperature.[44] This is likely due to its low solubility. Functionalizing the hypervalent iodine with acetate or trifluoroacetate leads to a significant improvement in yield under much milder conditions.[45] These reagents are commercially available, but are used stoichiometrically and are not readily recovered, reoxidized and reused. Polymer-supported hypervalent iodine reagents have overcome this issue, allowing for ready recovery and reuse.[46,47] Fluorinated alkyl chains appended either directly to the hypervalent I of pendant to an aryl iodide have allowed for the recovery and reuse of these efficient reagents as a result of their ready partitioning into fluorinated solvents following the reaction.[48,49] The magnetic Fe_3O_4 nanoparticle-supported hypervalent iodine was the first successful example of a recyclable hybrid iodine/metal catalyst. Here yields of over 80% were reported for the oxidation of hydroquinone with efficient recovery of the catalyst through a magnetic separation.[25] It should be noted that this system requires 2,2,2-trifluoroethanol as a solvent, and increasing reaction times with each recycle to maintain efficiency. The MOF-based systems reported in this study have the advantages of being catalytic, being readily recovered by filtration or centrifugation, proceeding under mild conditions, and working in a variety of solvents.

Table 8. Comparison of alkyl and aryl iodide-based catalysts and reagents for the oxidation of hydroquinone.

Catalyst/Reagent	Loading	Solvent	Time (min)	Temp. (°C)	Yield (%)
PhI=O[44]	2 eq.	Acetone/DCE	10	90	61
PhI(OAc)$_2$[45]	1 eq.	MeOH	N/A	RT	94
ArI(OAc)$_2$[b, c, 48]	1.2 eq.	MeOH	120-180	RT	95
RI(O$_2$CCF$_3$)$_2$[b, c, 49]	1 eq.	MeOH	10	RT	>99
Polymer supported PhI(OAc)$_2$[b, 50]	1.3 eq.	MeOH	240	RT	96
Polymer supported PhI(OAc)$_2$[b, 46]	2 eq.	MeOH	480	60	>99
Fe$_3$O$_4$ NPs supported iodoarene[25]	10 mol%[b]	CF_3CH_2OH/H_2O	30	RT	81
UiO-66 25%-I[a]	20 mol%	MeOH	2	50	92
MIL-53 25%-I[a]	20 mol%	CH_3NO_2/H_2O	60	50	70

a) The synthesized catalysts in this work.

b) Reagents can be recovered and reused

c) Ar represents arene with fluorinated alkyl chains, R represents fluorinated alkyl chain

CONCLUSIONS

Iodine is readily incorporated into Al and Zr MOFs by covalent modification of the linkers. The simple inclusion of the iodine element is not sufficient to guarantee a catalytically active site. Analysis of the structures revealed that there was insufficient space in the framework to accommodate reagents and oxidants. A multivariate approach was used to overcome this and allow for catalytic oxidation to occur within the MOF. The Al and Zr MOFs maintained their crystallinity over four recycles and only in the case where particle agglomeration was observed was there a notable loss in performance. XPS revealed that the oxidation states of the iodine sites were limited to +1 and +3. Future studies should augment the multivariate approach with a linker extension approach to increase the space in the pores to allow for more challenging substrates to be targeted. Furthermore, a longer linker should allow for the inclusion of I species that are known to achieve the +5 oxidation state or diiodine species that can bridge.

Conflicts of interest

There are no conflicts to declare.

ACKNOWLEDGMENT

The present work was support by the Robert A. Welch Foundation (D-1838, USA), Texas Tech University and from the National Science Foundation (NMR instrument grant CHE-

1048553). We are grateful for assistance from the Hope-Weeks group at Texas Tech for assistance with TGA measurements and the Jatib-Khatib group for assistance with surface area measurements.

References

1 A. Yoshimura and V. V. Zhdankin, *Chem. Rev.*, 2016, **116**, 3328–3435.
2 A. M. Harned, *Tetrahedron Lett.*, 2014, **55**, 4681–4689.
3 F. Berthiol, *Synthesis*, 2015, **47**, 587–603.
4 T. Dohi and Y. Kita, *Chem. Commun.*, 2009, 2073–2085.
5 J. Luiz F. Silva and B. Olofsson, *Nat. Prod. Rep.*, 2011, **28**, 1722–1754.
6 O. Prakash, D. Kumar, R. K. Saini and S. P. Singh, *Synth. Commun.*, 1994, **24**, 2167–2172.
7 P. A. Evans and T. A. Brandt, *J. Org. Chem.*, 1997, **62**, 5321–5326.
8 M. F. Greaney and W. B. Motherwell, *Tetrahedron Lett.*, 2000, **41**, 4467–4470.
9 *Org. Synth.*, 2006, **83**, 18.
10 T. Dohi, A. Maruyama, M. Yoshimura, K. Morimoto, H. Tohma and Y. Kita, *Angew. Chem. Int. Ed.*, 2005, **44**, 6193–6196.
11 M. Ochiai, Y. Takeuchi, T. Katayama, T. Sueda and K. Miyamoto, *J. Am. Chem. Soc.*, 2005, **127**, 12244–12245.
12 A. P. Thottumkara, M. S. Bowsher and T. K. Vinod, *Org. Lett.*, 2005, **7**, 2933–2936.
13 A. Schulze and A. Giannis, *Synthesis*, 2006, **2006**, 257–260.
14 M. Ochiai and K. Miyamoto, *Eur. J. Org. Chem.*, 2008, **2008**, 4229–4239.
15 V. V. Zhdankin and P. J. Stang, *Chem. Rev.*, 2008, **108**, 5299–5358.
16 A. Ozanne, L. Pouységu, D. Depernet, B. François and S. Quideau, *Org. Lett.*, 2003, **5**, 2903–2906.
17 M. Frigerio and M. Santagostino, *Tetrahedron Lett.*, 1994, **35**, 8019–8022.
18 P. T. Anastas, I. J. Levy and K. E. Parent, *Green Chemistry Education: Changing the Course of Chemistry*, American Chemical Society, 2009.
19 P. I. Dalko and L. Moisan, *Angew. Chem. Int. Ed.*, 2004, **43**, 5138–5175.
20 H. Pellissier, *Tetrahedron*, 2007, **63**, 9267–9331.
21 C. A. McNamara, M. J. Dixon and M. Bradley, *Chem. Rev.*, 2002, **102**, 3275–3300.
22 P. Hodge, *Curr. Opin. Chem. Biol.*, 2003, **7**, 362–373.
23 N.-H. Nam, S. Sardari and K. Parang, *J. Comb. Chem.*, 2003, **5**, 479–546.
24 G. Sorg, A. Mengel, G. Jung and J. Rademann, *Angew. Chem. Int. Ed.*, 2001, **40**, 4395–4397.
25 M. Mülbaier and A. Giannis, *Angew. Chem. Int. Ed.*, 2001, **40**, 4393–4394.
26 N. N. Reed, M. Delgado, K. Hereford, B. Clapham and K. D. Janda, *Bioorg. Med. Chem. Lett.*, 2002, **12**, 2047–2049.
27 Y.-H. Kim, H.-S. Jang, Y.-O. Kim, S.-D. Ahn, S. Yeo, S.-M. Lee and Y.-S. Lee, *Synlett*, 2013, **24**, 2282–2286.
28 Nambu Hisanori, Shimokawa Ikumi, Fujiwara Tomoya and Yakura Takayuki, *Asian J. Org. Chem.*, 2016, **5**, 486–489.
29 A. H. Chughtai, N. Ahmad, H. A. Younus, A. Laypkov and F. Verpoort, *Chem. Soc. Rev.*, 2015, **44**, 6804–6849.
30 J. H. Cavka, S. Jakobsen, U. Olsbye, N. Guillou, C. Lamberti, S. Bordiga and K. P. Lillerud, *J. Am. Chem. Soc.*, 2008, **130**, 13850–13851.
31 T. Loiseau, C. Serre, C. Huguenard, G. Fink, F. Taulelle, M. Henry, T. Bataille and G. Férey, *Chem. – Eur. J.*, 2004, **10**, 1373–1382.
32 S. M. Chavan, G. C. Shearer, S. Svelle, U. Olsbye, F. Bonino, J. Ethiraj, K. P. Lillerud and S. Bordiga, *Inorg. Chem.*, 2014, **53**, 9509–9515.
33 L. Ma, J. M. Falkowski, C. Abney and W. Lin, *Nat. Chem.*, 2010, **2**, 838–846.
34 O. M. Fugaeva, I. K. Korobeinicheva and V. V. Bardin, *Bull. Acad. Sci. USSR Div. Chem. Sci.*, 1991, **40**, 2309–2311.
35 A. D. Burrows, L. C. Fisher, C. Richardson and S. P. Rigby, *Chem. Commun.*, 2011, **47**, 3380–3382.
36 X. Wang and A. J. Jacobson, *J. Solid State Chem.*, 2016, **236**, 230–235.
37 L. Valenzano, B. Civalleri, S. Chavan, S. Bordiga, M. H. Nilsen, S. Jakobsen, K. P. Lillerud and C. Lamberti, *Chem. Mater.*, 2011, **23**, 1700–1718.
38 G. Ortiz, G. Chaplais, J.-L. Paillaud, H. Nouali, J. Patarin, J. Raya and C. Marichal, *J. Phys. Chem. C*, 2014, **118**, 22021–22029.
39 B. V. de Voorde, I. Stassen, B. Bueken, F. Vermoortele, D. D. Vos, R. Ameloot, J.-C. Tan and T. D. Bennett, *J. Mater. Chem. A*, 2014, **3**, 1737–1742.
40 Z. Bastl and H. Gehlmann, *Collect. Czechoslov. Chem. Commun.*, 1988, **53**, 425–432.
41 E. Guibal, T. Vincent, E. Touraud, S. Colombo and A. Ferguson, *J. Appl. Polym. Sci.*, 2006, **100**, 3034–3043.
42 X.-Q. Zhu, C.-H. Wang and H. Liang, *J. Org. Chem.*, 2010, **75**, 7240–7257.
43 Y.-C. Lai, C.-W. Kung, C.-H. Su, K.-C. Ho, Y.-C. Liao and D.-H. Tsai, *Langmuir*, 2016, **32**, 6123–6129.
44 W. Yang, S. Wang, Q. Zhang, Q. Liu and X. Xu, *Chem. Commun.*, 2014, **51**, 661–664.
45 A. Pelter and S. Elgendy, *Tetrahedron Lett.*, 1988, **29**, 677–680.
46 S. Ficht, M. Mülbaier and A. Giannis, *Tetrahedron*, 2001, **57**, 4863–4866.
47 Y. Shang, T. Y. S. But, H. Togo and P. H. Toy, *Synlett*, 2007, **2007**, 0067–0070.
48 Rocaboy Christian and Gladysz John A., *Chem. – Eur. J.*, 2002, **9**, 88–95.
49 V. Tesevic and J. A. Gladysz, *Green Chem.*, 2005, **7**, 833–836.
50 Y. Shang, T. Y. S. But, H. Togo and P. H. Toy, *Synlett*, 2007, **2007**, 0067–0070.